Phase-field modelling for atoms

Kairi Masuda*

Department of Mechanical Engineering and Science, Kyoto University, Nishikyo-ku, Kyoto 615-8540, Japan

E-mail: masuda.kairi.64n@st.kyoto-u.ac.jp

Abstract

The application of phase-field modelling has been expanded into smaller and smaller-scale phenomena. However, phase-field modelling with a single atomic resolution has not been proposed so far. Here, we have developed atomic-scale phase-field modelling, that is, phase-field modelling for single atoms. We found that our modelling successfully reproduced the stabilization of Cu lattices under NVT and NPT conditions. Moreover, we found that our modelling allows us to use a longer time step than MD simulations to simulate atom dynamics. This research expands the application of phase-field simulation into the ultra-small scale, providing a powerful strategy to clarify atomic but longer time-scale phenomena.

Introduction

In phase-field modelling, an interface is modelled as a continuous field and its dynamics are calculated by solving diffusion equations. This methodology has achieved great success for mesoscopic materials properties in a diffusive time scale such as solidification, fracture, and ferroelectricity [1–3]. As one direction of the developments, the application of phase-field simulation has gradually expanded to a smaller scale. For example, phase-field simulation of

dislocation dynamics, coupling between ferroelectricity and dislocations, and thermal activated skyrmion motions has been conducted [4–6]. Such developments of phase-field simulations have undoubtedly clarified many material properties at the nanoscale but diffusive time scale where molecular dynamics (MD) and quantum mechanical simulations can not access.

In this context, phase-field crystal modelling has been proposed, in which the crystallines of material are represented by periodic fields such as trigonometric functions [7–10]. In this modelling, each peak of a wave corresponds to the probability density of atom vibration. In other words, the application of phase-field simulation has now reached the quasi-atomic-scale. This concept is novel because they show that phase-field modelling has the ability to investigate diffusive time-scale phenomena with atomic resolution. However, those phase-field modelling assumes crystallinity in solid states and this limitation restricts their simulation targets. In other words, if such a limitation can be removed, phase-field simulation will be applied not only to more complicated materials such as organic materials [11–14] but also to chemistry and biology, in which micro-millisecond phenomena have gained a lot of attention [15–17].

The purpose of this study is to develop atomic-scale phase-field modelling, that is, phase-field modelling for single atoms. In the following, we describe how to model atoms and calculate their dynamics. Then, we validate our modelling by comparing it with MD simulations. Furthermore, we investigate how much time step can be used in simulation to show the ability of our modelling for clarifying longer time scale phenomena. Finally, we summarize this study.

Methods

Theory

The thermal vibration of an atom around a mean position appears as a density cloud on a longer time scale. In many solids, since this vibration is narrow and isotropic, a probability density ρ of this atomic cloud can be approximated by a normalized Gaussian as follows

(Supplemental Information 1)

$$\rho_i(\boldsymbol{x}_i|\boldsymbol{X}_i,\alpha_i) = \left(\frac{\alpha_i}{\pi}\right)^{3/2} e^{-\alpha_i(\boldsymbol{x}_i-\boldsymbol{X}_i)^2}, \tag{1}$$

where $\boldsymbol{X}_i$ is the position of the vibration center of atoms i =1, 2, ..., N while α_i =$m_i\omega_i/2k_BT$ is a parameter related to temperature in which m_i is the atomic mass, ω_i is the Einstein frequency, k_B is the Boltzmann constant, and T is the absolute temperature. When $\boldsymbol{X}_i$ and α_i are given as a condition, a probability density at the position $\boldsymbol{x}_i$ is determined. The variational Gaussian (VG) theory says that the Helmholtz free energy for such probability densities can be described as follows[18,19]

$$F = \frac{3}{2}k_BT\sum_{i=1}^{N}\left\{\ln\left(\frac{\alpha_i\Lambda^2}{\pi}\right)-1\right\} + \frac{1}{2}\sum_{i=1}^{N}\sum_{j\neq i} w_{ij}(\boldsymbol{X}_i,\boldsymbol{X}_j,\alpha_i,\alpha_j). \tag{2}$$

The first term is energy for atom vibrations where $\Lambda = \hbar\sqrt{2\pi/m_ik_BT}$ is the de Broglie thermal wavelength. The second term is energy for interactions between probability densities and w_{ij} is an effective pair potential described as follows

$$\begin{aligned} w_{ij}(\boldsymbol{X}_i,\boldsymbol{X}_j,\alpha_i,\alpha_j) &= \int \rho_i(\boldsymbol{x}_i)\int \rho_j(\boldsymbol{x}_j)\phi(x_{ij})d\boldsymbol{x}_i d\boldsymbol{x}_j \\ &= \left(\frac{\alpha_i}{\pi}\right)^{3/2}\left(\frac{\alpha_j}{\pi}\right)^{3/2}\int e^{-\alpha_i(\boldsymbol{x}_i-\boldsymbol{X}_i)^2}\int e^{-\alpha_j(\boldsymbol{x}_j-\boldsymbol{X}_j)^2}\phi(x_{ij})d\boldsymbol{x}_i d\boldsymbol{x}_j, \end{aligned} \tag{3}$$

where $\boldsymbol{x}_{ij} = \boldsymbol{x}_j - \boldsymbol{x}_i$, $x_{ij} = |\boldsymbol{x}_{ij}|$, and ϕ is a pair potential between atoms. To understand this potential, remind that an electric potential $\phi(x) = q/x$ by a point charge q corresponds with $\phi(x) = \int q\rho(x')/(x-x')dx'$ by charge density ρ. This potential is equal to the following

form (Supplemental Information 2)[20]

$$
\begin{aligned}
w_{ij}(X_{ij},\alpha_{ij}) &= \left(\frac{\alpha_{ij}}{\pi}\right)^{3/2}\int e^{-\alpha_{ij}(\boldsymbol{x}_{ij}-\boldsymbol{X}_{ij})^2}\phi(x_{ij})d\boldsymbol{x}_{ij} \\
&= 2\pi\left(\frac{\alpha_{ij}}{\pi}\right)^{3/2}\int_0^{r_c}\int_0^{\pi} r^2 dr d\theta \sin\theta \\
&\quad \times e^{-\alpha_{ij}r^2}\phi(\sqrt{r^2+X_{ij}^2+2rX_{ij}\cos\theta}),
\end{aligned}
\tag{4}
$$

where $\boldsymbol{X}_{ij} = \boldsymbol{X}_j - \boldsymbol{X}_i$, $X_{ij} = |\boldsymbol{X}_{ij}|$, $\alpha_{ij} = (1/\alpha_i + 1/\alpha_j)^{-1}$, and r_c is the cutoff on the Gaussian. This form is convenient to calculate an effective potential energy.

In previous studies[18–20], the authors just optimized the above free energy to obtain finite-temperature equilibrium states and they did not use it for dynamics. In this study, we use the above theory for dynamics in the framework of the phase-field method. In other words, based on the above free energy and Cahn-Hilliard equation[3], we obtain the following governing equation

$$
\begin{aligned}
\frac{\partial\rho_i(\boldsymbol{x},t)}{\partial t} &= \nabla\left(D_i(\boldsymbol{x})\nabla\frac{\delta F}{\delta\rho_i}\right) \\
&= \nabla(\kappa_i\rho_i(\boldsymbol{x})\nabla\Phi_i(\boldsymbol{x})),
\end{aligned}
\tag{5}
$$

where t is time and $D_i(\boldsymbol{x})$ is a position-dependent kinetic coefficient. Here, as κ_i is a kinetic coefficient, we consider $D_i(\boldsymbol{x}) = \kappa_i\rho_i(\boldsymbol{x})$ because a probability density should follow the conservation law. Here, a differential of functional derivative $\nabla\delta F/\delta\rho_i = \nabla\Phi_i(\boldsymbol{x})$ is an effective force described as follows

$$
\nabla\Phi_i(\boldsymbol{x}) = \sum_{j\neq i}\int e^{-\alpha_j(\boldsymbol{x}_j-\boldsymbol{X}_j)^2}\nabla\phi(|\boldsymbol{x}-\boldsymbol{x}_j|)d\boldsymbol{x}_j. \tag{6}
$$

By solving the above governing equation and force, the motion of probability densities should be calculated.

Simulation detail

To test the above theory, we employed Cu metals (m = 63.55 g/mol). A pairwise Morse potential of Cu can be described as follows[18]

$$\phi(x_{ij}) = D_0\{e^{-2\beta(x_{ij}-x_0)} - 2e^{-\beta(x_{ij}-x_0)}\} \tag{7}$$

where D_0 = 0.3429 eV, β = 1.3588 Å^{-1}, and x_0 = 2.866 Å while the cutoff distance is 8 Å. As the initial structure, we considered 2 × 2 × 2 cells with a lattice constant a_0 = 3.61Å, that is, the box size of 7.22 Å × 7.22 Å × 7.22 Å. In this box, we arranged 32 Cu atoms to the face-centred-cubic (FCC) positions with random displacements between -0.1 and 0.1 Å in the x, y, and z directions. Then, we applied periodic boundary conditions to this structure. To validate the above theory, we calculated the time development of this structure under the constant volume and temperature (NVT) condition from both phase-field and MD simulations.

For phase-field simulation, Eq. (5) has the same form as the Fokker-Planck equation described as

$$\frac{\partial \rho_i(\boldsymbol{x}, t)}{\partial t} = \nabla(\boldsymbol{a}_i(\boldsymbol{x})\rho_i(\boldsymbol{x})), \tag{8}$$

where $\boldsymbol{a}$ is a drift coefficient. Since the Fokker-Plank equation can be converted into the Langevin equation, this can be converted as follows (Supplemental Information 3)[21]

$$\frac{d\boldsymbol{X_i}}{dt} = -\boldsymbol{a}_i(\boldsymbol{X_i}) = -\nabla\Phi_i(\boldsymbol{X_i}). \tag{9}$$

By solving this equation by the Vervet algorithm (Supplemental Information 4) with the time step Δt = 1 fs, we calculated the motions of the centres of probability densities. On the other hand, the calculation of effective potential energy and force (Eqs. (4) and (6)) every time step increases computational costs because they include integrals. Therefore, we made lookup tables for the effective pair potential and force until the cutoff distance with

0.01 Å interval. For α, we calculated them by optimizing Eq. (2) by L-BFGS under 1 GPa (Supplemental Information 1)[22,23], and the obtained values are summarized in Table 1. Note that, since $\alpha = 1/2\sigma^2$ where σ is a standard deviation of Gauss distribution, $\alpha = \infty$ and $F = 1/2 \sum_{i=1}^{N} \sum_{j \neq i} \phi(X_{ij})$ at 0 K. For the mobility, a conductivity $\kappa = 5.56 \times 10^{-8}$ m^2/(V$\cdot$ s) was taken from the mobility of Cu^{2+} in water at 298 K[24].

For MD, we used LAMMPS software[25] to calculate the time development of the above initial structure under NVT the same as the phase-field simulation. We applied an initial velocity corresponding to 300 K and the temperatue is controlled by the Berendsen thermostat. Then, we calculated 20000 steps with the time step being 1 fs. Values such as pressure are calculated in each time step.

Table 1: Values of α used in this study, which are obtained by optimising Eq. (2) by L-BFGS under 1 GPa.

	0 K	300 K	600 K	900 K	1200 K
α (Å^{-2})	∞	240.9	120.0	78.3	57.8

Results

Time development

Figure 1 shows a typical time development of Cu atoms under 300 K by phase-field simulation. Note that atoms are represented by clouds to emphasize that we treat a probability density. Moreover, atoms at the face-centred positions are represented by a blighter colour for clarity. We found that atoms, which are displaced randomly as the initial condition (Fig. 1(a)), move toward the equilibrium fcc position as time passes (Fig. 1(b)). Finally, the positions of atoms almost return to the fcc positions at $t = 25$ fs (Fig. 1(c)). Therefore, our phase-field simulation has the ability to reproduce the equilibrium state of Cu.

Then, we calculated the time development of the pressure of the above system. We derived the pressure P of the system from the Helmholtz free energy as follows

$$P = -\Big(\frac{\partial F}{\partial V}\Big)_{T,N} = -\frac{1}{2}\sum_i \sum_{j\neq i} \frac{\partial \omega(X_{ij})}{\partial X_{ij}} \frac{\partial X_{ij}}{\partial V} = \frac{1}{2}\sum_i \sum_{j\neq i} f_{ij} \frac{X_{ij}}{3V} \tag{10}$$

where V is the volume of the system and $f_{ij} = -\partial\omega(X_{ij})/\partial X_{ij}$ is a force between probability densities i and j. $\partial X_{ij}/\partial V = X_{ij}/3V$ can be derived from the scaling of the system (Supplemental Information 5). This indicates that pressure can be calculated by virial (= force $\times$ distance) the same as MD simulations. Figure 2 shows the time development of pressure calculated by the above equation (red line). For comparison, a pressure calculated by MD is also plotted (black line). We found that pressures in both phase-field and MD simulations reach the equilibrium pressure through a similar steep descent behaviour. The equilibrium pressure value is 2.18 GPa in phase-field simulation and 1.96 GPa in MD simulation. In other words, a pressure value by phase-field simulation is comparative with that by MD simulation. Thus, we concluded that our modelling successfully reproduced the time development of pressure.

Figure 3 shows the variation of the equilibrium pressure by temperature difference under

the NVT condition obtained by phase-field and MD simulations. Detailed values for each simulation are listed in Table 2. We found that the equilibrium pressures by both simulations show a similar trend, that is, almost linear incrementation. On the other hand, we also found that the discrepancy of pressures between simulations expands as temperature increases. The reason can be attributed that we employed α values obtained under 1 GPa. That is, the deviation from 1 GPa increases by raising the temperature under the NVT condition, changing the α values we should use. Moreover, at high-temperature regions, a slight change of α will make a large subsequent difference because α converges as shown in Fig. S2. Therefore, high-temperature conditions should be avoided in our phase-field modelling if a large pressure fluctuation is expected.

Table 2: The equilibrium pressure under the NVT condition obtained by phase-field and MD simulations.

Temperature (K)	Phase-field (GPa)	MD (GPa)
0	0.74	0.71
300	2.18	1.96
600	3.65	3.22
900	5.22	4.56
1200	6.85	6.01

Stress control

Then, we considered the constant temperature and pressure (NPT) condition. For this, we change the volume of the system by the following equation[26]

$$\frac{dV}{dt} = M(P - P_0), \tag{11}$$

where P_0 is an applied external pressure and M is mobility of the volume. In other words, we scale the positions and volume at each time step as follows

$$\begin{aligned} \boldsymbol{X_i} &\rightarrow \mu \boldsymbol{X_i}, \\ V &\rightarrow \mu^3 V, \end{aligned} \tag{12}$$

where μ is a scale factor, which is described as follows

$$\mu = \{1 + M' \Delta t (P - P_0)\}^{\frac{1}{3}}, \tag{13}$$

where $M' = M/V$ is mobility of a scale factor.

By the above pressure and volume control, we calculated the equilibrium lattice constants by phase-field simulation. We used the same parameters and initial structure as the above NVT conditions. For the mobility of a scale factor, we used $M' = 10$ in this study. For comparison, we conducted the same calculation by MD simulation using the LAMMPS software(we used the dump = 2 commands to suppress fluctuation). Figure 4 shows the obtained time developments of lattice constants by phase-field and MD simulations under $P_0 = 1$ GPa and $T = 300$ K. We found that both simulations converge to the almost same equilibrium lattice constant as time passes. Therefore, we concluded that pressure and volume controls can be conducted by the above equation in our phase-field simulations.

Figure 5 is the temperature dependence of a lattice constant after equilibrium under $P_0 = 0$, 1, and 10 GPa obtained by phase-field and MD simulations. Detailed values for each simulation are listed in Table 3. We found that lattice constants agree with the MD simulation under moderate pressure (Figs. 5(a) and (b)). This is also applied to the results under high pressure and moderate temperatures ($T < 600$K in Fig. 5(c)). Therefore, our modelling successfully reproduced the temperature-dependent lattice constants of Cu. On the other hand, under high pressure and high temperature, a discrepancy between MD and phase-field simulations increases ($T > 600$ K in Fig. 5(c)). This result agrees with the above

discussion, that is, a slight change of α by a large pressure makes a large difference in related properties in high-temperature regions. Thus, we again say that high temperature and large pressure conditions should be avoided in our phase-field modelling.

Table 3: The equilibrium lattice constants under the NPT condition obtained by phase-field and MD simulations.

Pressure (GPa)	Temperature (K)	phase-field (Å)	MD (Å)
0	0	3.616	3.616
	300	3.628	3.628
	600	3.641	3.639
	900	3.654	3.653
	1200	3.667	3.665
1	0	3.608	3.608
	300	3.620	3.618
	600	3.632	3.630
	900	3.645	3.643
	1200	3.658	3.655
10	0	3.540	3.539
	300	3.550	3.549
	600	3.562	3.558
	900	3.573	3.567
	1200	3.588	3.577

Allowable time step

In the above, we set the time step $\Delta t = 1$ fs in phase-field simulations to compare the results with MD simulations. However, since we do not need to consider atom vibration when atoms are treated as a probability density, we may be able to use larger time steps for calculations. Thus, we recalculated the above NVT and NPT simulations with different Δt to investigate the allowable time step for the calculation. Figure 6(a) shows the recalculated time development of pressure under the NVT condition of $a_0 = 3.61$ Å and $T = 300$ K with $\Delta t = 1$, 10, and 100 fs. We found that the same time development as $\Delta t = 1$ fs is obtained by $\Delta t = 10$ fs. More surprisingly, a pressure converges to the same value even by $\Delta t = 100$ fs although there is a slight deviation in the convergence path (the enlarged view in Fig. 6(a)).

This is also applied to the calculation under the NPT condition (Fig. 6(b)). Therefore, we can use several ten femtosecond or more longer time steps to obtain the same results as those by 1 fs. This suggests that atomic-scale phase-field simulation will be a powerful strategy to investigate atomic-scale but longer time-scale phenomena that are difficult for MD simulation.

Conclusion

In summary, we have developed atomic-scale phase-field modelling, in which atom vibrations are modelled as a Gauss distribution. Our modelling successfully reproduced the stabilization of Cu lattices under NVT and NPT conditions. Furthermore, we found that our phase-field modelling allows us to use longer time steps than MD simulations to calculate dynamics. This methodology will be a powerful strategy to investigate atomic but longer time-scale phenomena that are difficult for MD simulations.

Acknowledgement

This work was supported by JSPS KAKENHI grant numbers 21J10412.

Supporting Information Available

The Supporting Information is available free of charge at

- PDF: Distribution of atom vibration (Figs. S1 and S2), Transformation of multiple integral (Fig. S3), Transformation of the governing equation (Fig. S4), The Verlet algorithm for a diffusive equation, and The differential of distance with respect to volume.

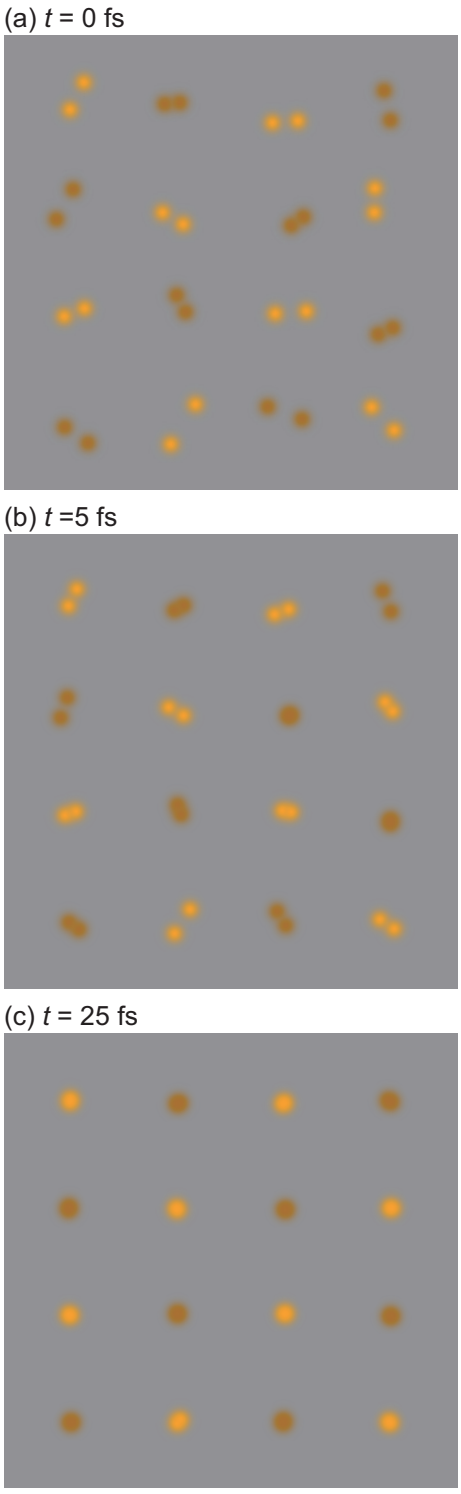

Figure 1: The time development of Cu atoms obtained by phase-field simulation under the NVT condition of a lattice constant $a_0 = 3.61$ Å and $T = 300$ K. To emphasise we treat probability densities, atoms are represented by clouds. For the eye guide, atoms at the face-centred positions are represented by a blighter colour.

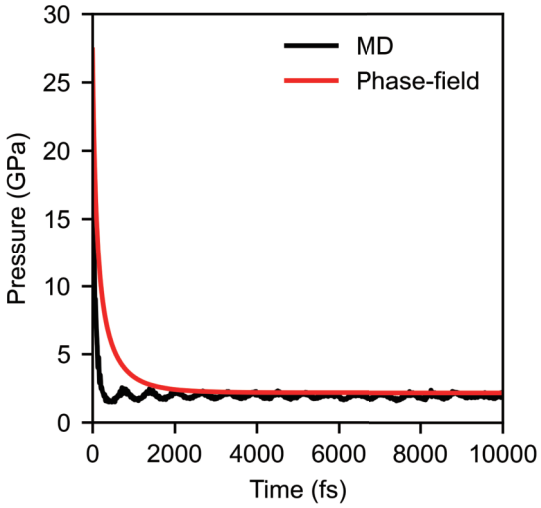

Figure 2: The time development of pressure under the NVT condition obtained by atom motions in Fig. 1. The corresponding result by MD simulation is also plotted for comparison by a black line.

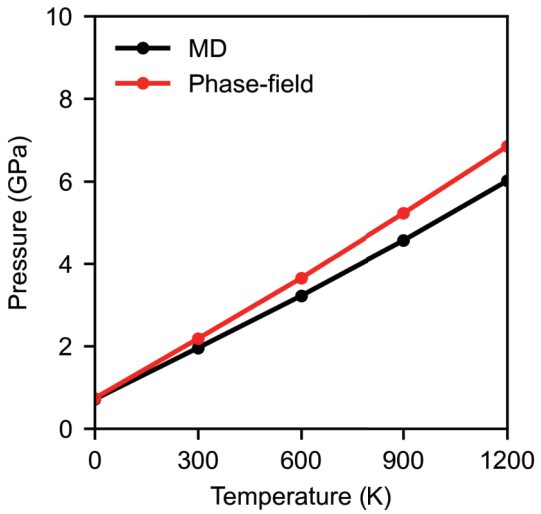

Figure 3: Temperature dependence of the equilibrium pressure under the NVT condition.

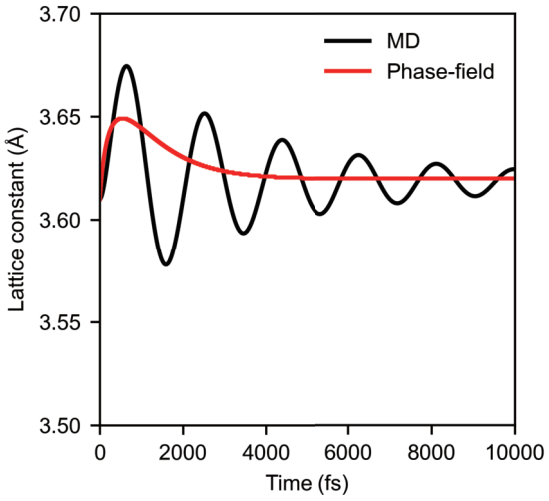

Figure 4: The time developments of lattice constants of Cu by phase-field and MD simulations under the NPT condition of $P_0 = 1$ GPa and $T = 300$ K.

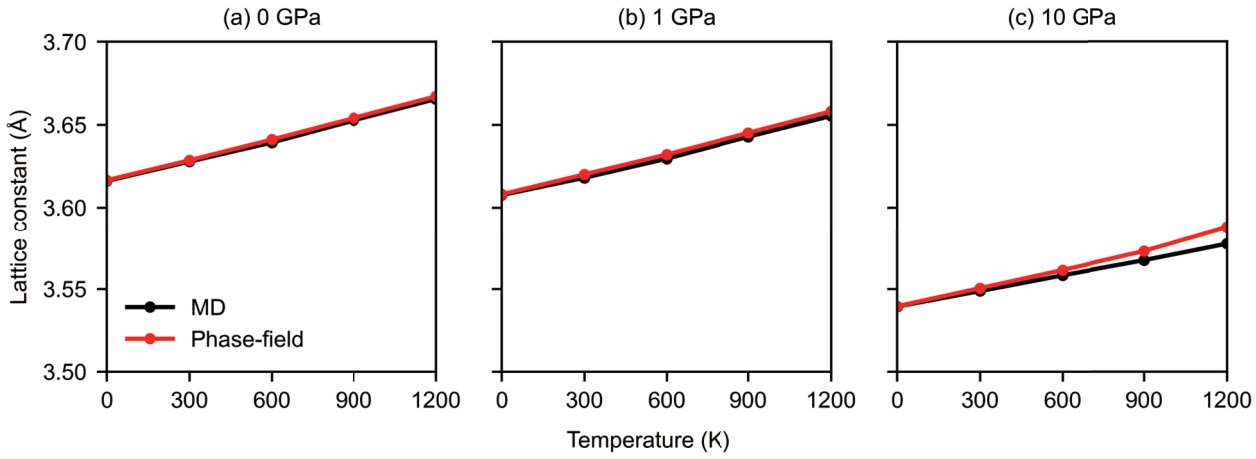

Figure 5: Temperature dependence of the equilibrium lattice constants obtained by phase-field and MD simulations for $P_0 =$ (a) 0 GPa, (b) 1 GPa, and (c) 10 GPa.

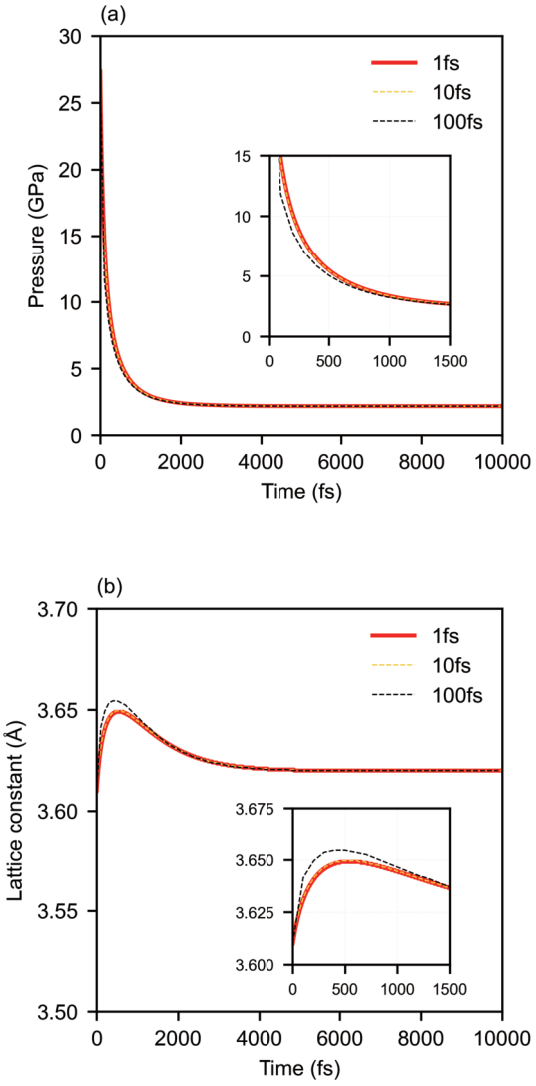

Figure 6: Recalculated time developments of (a) pressure under the NVT condition of $a_0 = 3.61$Å and $T = 300$ K, and (b) lattice constants under the NPT condition of $P_0 = 1$ GPa and T = 300 K with different time steps.

References

(1) Boettinger, W. J.; Warren, J. A.; Beckermann, C.; Karma, A. Phase-Field Simulation of Solidification. *Annu. Rev. Mater. Res.* **2002**, *32*, 163–194.

(2) Ambati, M.; Gerasimov, T.; De Lorenzis, L. A Review on Phase-Field Models of Brittle Fracture and a New Fast Hybrid Formulation. *Comput. Mech.* **2015**, *55*, 383–405.

(3) Chen, L. Q. Phase-Field Models for Microstructure Evolution. *Annu. Rev. Mater. Res.* **2002**, *32*, 113–140.

(4) Wang, Y. U.; Jin, Y. M.; Cuitiño, A. M.; Khachaturyan, A. G. Nanoscale Phase Field Microelasticity Theory of Dislocations: Model and 3D Simulations. *Acta Mater.* **2001**, *49*, 1847–1857.

(5) Masuda, K.; Lich, L. V.; Shimada, T.; Kitamura, T. Periodically-Arrayed Ferroelectric Nanostructures Induced by Dislocation Structures in Strontium Titanate. *Phys. Chem. Chem. Phys.* **2019**, *21*, 22756–22762.

(6) Wang, Y.; Kitamura, T.; Wang, J.; Hirakata, H.; Shimada, T. Mechanical Acceleration and Control of the Thermal Motion of a Magnetic Skyrmion. *Phys. Rev. Applied* **2022**, *18*, 014049.

(7) Elder, K. R.; Grant, M. Modeling Elastic and Plastic Deformations in Nonequilibrium Processing Using Phase Field Crystals. *Phys. Rev. E* **2004**, *70*, 051605.

(8) Chan, P. Y.; Goldenfeld, N.; Dantzig, J. Molecular Dynamics on Diffusive Time Scales from the Phase-Field-Crystal Equation. *Phys. Rev. E* **2009**, *79*, 035701.

(9) Berry, J.; Grant, M.; Elder, K. R. Diffusive Atomistic Dynamics of Edge Dislocations in Two Dimensions. *Phys. Rev. E* **2006**, *73*, 031609.

(10) Provatas, N.; Dantzig, J. A.; Athreya, B.; Chan, P.; Stefanovic, P.; Goldenfeld, N.; Elder, K. R. Using the Phase-Field Crystal Method in the Multi-Scale Modeling of Microstructure Evolution. *JOM* **2007**, *59*, 83–90.

(11) Yamamoto, T. Computer Modeling of Polymer Crystallization – Toward Computer-Assisted Materials' Design. *Polymer* **2009**, *50*, 1975–1985.

(12) Horiuchi, S.; Tokura, Y. Organic Ferroelectrics. *Nat. Mater.* **2008**, *7*, 357–366.

(13) Liu, Y.; Cai, H. L.; Zelisko, M.; Wang, Y.; Sun, J.; Yan, F.; Ma, F.; Wang, P.; Chen, Q. N.; Zheng, H.; Meng, X.; Sharma, P.; Zhang, Y.; Li, J. Ferroelectric Switching of Elastin. *Proc. Natl. Acad. Sci. U.S.A.* **2014**, *111*, E2780–E2786.

(14) Zhao, G.; Perilla, J. R.; Yufenyuy, E. L.; Meng, X.; Chen, B.; Ning, J.; Ahn, J.; Gronenborn, A. M.; Schulten, K.; Aiken, C.; Zhang, P. Mature HIV-1 Capsid Structure by Cryo-Electron Microscopy and All-Atom Molecular Dynamics. *Nature* **2013**, *497*, 643–646.

(15) Lindorff-Larsen, K.; Piana, S.; Dror, R. O.; Shaw, D. E. How Fast-Folding Proteins Fold. *Science* **2011**, *334*, 517–520.

(16) Hamelberg, D.; Mongan, J.; McCammon, J. A. Accelerated Molecular Dynamics: A Promising and Efficient Simulation Method for Biomolecules. *J. Chem. Phys.* **2004**, *120*, 11919–11929.

(17) Jung, J.; Mori, T.; Sugita, Y. Efficient Lookup Table Using a Linear Function of Inverse Distance Squared. *J. Comput. Chem.* **2013**, *34*, 2412–2420.

(18) LeSar, R.; Najafabadi, R.; Srolovitz, D. J. Finite-Temperature Defect Properties from Free-Energy Minimization. *Phys. Rev. Lett.* **1989**, *63*, 624–627.

(19) LeSar, R.; Najafabadi, R.; Srolovitz, D. J. Thermodynamics of Solid and Liquid

Embedded-Atom-Method Metals: A Variational Study. *J. Chem. Phys.* **1991**, *94*, 5090–5097.

(20) Li, J.; Sarkar, S.; Cox, W. T.; Lenosky, T. J.; Bitzek, E.; Wang, Y. Diffusive Molecular Dynamics and Its Application to Nanoindentation and Sintering. *Phys. Rev. B* **2011**, *84*, 054103.

(21) Uhlenbeck, G. E.; Ornstein, L. S. On the Theory of the Brownian Motion. *Phys. Rev.* **1930**, *36*, 823–841.

(22) Nocedal, J. Updating Quasi-Newton Matrices with Limited Storage. *Math. Comput.* **1980**, *35*, 773–782.

(23) Virtanen, P. et al. SciPy 1.0: Fundamental Algorithms for Scientific Computing in Python. *Nat. Methods* **2020**, *17*, 261–272.

(24) Harris, D. C. *Quantitative Chemical Analysis*, 8th ed.; W. H. Freeman and Company: New York, 2010; p 314.

(25) Thompson, A. P.; Aktulga, H. M.; Berger, R.; Bolintineanu, D. S.; Brown, W. M.; Crozier, P. S.; in 't Veld, P. J.; Kohlmeyer, A.; Moore, S. G.; Nguyen, T. D.; Shan, R.; Stevens, M. J.; Tranchida, J.; Trott, C.; Plimpton, S. J. LAMMPS - a Flexible Simulation Tool for Particle-Based Materials Modeling at the Atomic, Meso, and Continuum Scales. *Comput. Phys. Commun.* **2022**, *271*, 108171.

(26) Kocher, G.; Provatas, N. New Density Functional Approach for Solid-Liquid-Vapor Transitions in Pure Materials. *Phys. Rev. Lett.* **2015**, *114*, 155501.